Novel reduced-order modeling method combined with three-particle nonlinear transform unscented Kalman filtering for the battery state-of-charge estimation.

XU, W., WANG, S., FERNANDEZ, C., YU, C., FAN, Y. and CAO, W.

2020

Novel reduced-order modeling methods combined with three-particle nonlinear transform unscented Kalman filtering for the battery state-of-charge estimation

Wenhua Xu[1] · Shunli Wang[1*] · Carlos Fernandez[2] · Chunmei Yu[1] · Yongcun Fan[1] · Wen Cao[1]

1 School of Information Engineering, Southwest University of Science and Technology, Mianyang, China.
***Shunli Wang: 497420789@qq.com**
2 School of Pharmacy and Life Sciences, Robert Gordon University, Aberdeen, SCT, UK

Abstract

Accurate estimation of the lithium-ion battery state of charge plays an important role in the real-time monitoring and safety control of batteries. In order to solve the problems that the real-time estimation of the lithium-ion battery is difficult and the estimation accuracy is not high under various working conditions, a lithium-ion battery is taken as a research object, and the working characteristics of the lithium-ion battery are studied under various working conditions. In order to reduce the computational complexity of the traditional unscented Kalman algorithm, an improved unscented Kalman algorithm is proposed. Considering the importance of accurately estimating the initial state of charge for later estimation, the initial estimation value is calibrated by using the open-circuit voltage method. Then, the improved unscented Kalman filter algorithm based on a reduced-order model is used for assessing and tracking to realize real-time high-precision estimation of the state of charge of the lithium-ion battery. A simulation model is built and combined with a variety of working conditions data for performance analysis. The experimental results show that the convergence speed and tracking effect are good and that the estimation error control is within 0.8%. It is verified that the reduced order of the three-particle nonlinear transform unscented Kalman results in higher accuracy in the state-of-charge estimation of lithium-ion batteries.

Keywords: Lithium-ion battery · Thevenin model · State of charge · Unscented Kalman filtering algorithm · Nonlinear transform

1 Introduction

Energy security and environmental protection play an important role in the development plan of the world's economy. Pursuing new energy sources to replace traditional fossil fuels has become a focus of attention worldwide [1]. Lithium-ion batteries have been widely used and developed in the field of new energy due to their high energy density, high output power and high-cost performance [2]. With the wide application of lithium-ion batteries in the field of new energy, their health condition detection has received increasing attention. It is of great importance to accurately estimate the state of charge (SOC) of lithium-ion batteries for maximizing their performance and for realizing real-time state detection and safety control of lithium-ion batteries [3]. Lithium-ion batteries are often used under complex working conditions, and their state detection is susceptible to environmental noise [4, 5]. Moreover, the internal electrochemical reaction of the lithium-ion battery is complicated and is often accompanied by polarization effects and ohmic effects [6, 7]. The interference of other factors makes it difficult for traditional algorithms to obtain accurate real-time SOC estimation of the lithium-ion battery [8, 9]. Therefore, a method to establish an equivalent model of a battery and to use correct and appropriate algorithms to estimate the SOC of a battery is of great significance for the real-time monitoring and safety control of lithium batteries. This is also important for improving battery efficiency. Researchers have done a

great deal of work on this [10–13]. In the SOC estimation process of the lithium-ion battery, the construction of a battery equivalent model occupies an important position [14, 15]. Common battery models in current applications include electrochemical [16], neural network and equivalent circuit models [17–19]. The equivalent circuit model uses circuit knowledge to establish circuit equations to study the battery characteristics, and the resulting convenience has been widely used in the engineering field. At present, the commonly used methods in the estimation of the lithium-ion battery SOC are the open-circuit voltage (OCV) method, the Ampere-hour (Ah) integral method, the neural network method and the Kalman filter (KF) method [20–23]. The open-circuit voltage method uses the correspondence between the OCV and the SOC to obtain the SOC value [24, 25]. The Ah integral method uses the definition to calculate the SOC by integrating the current. The Kalman filter method obtains the optimal solution in terms of minimum variance through continuous iterative operations [26]. Due to the complex electrochemical reactions of batteries during use, they often exhibit strong nonlinear characteristics. In addition, there are some defects in traditional algorithms. Thus, the above methods are unable to accurately estimate the SOC of lithium-ion batteries. In recent years, researchers have proposed some improved algorithms based on traditional algorithms to solve the problems of the difficult and low online estimation accuracy of lithium-ion batteries [27–33]. They used different algorithms to estimate and improve the SOC. However, they did not consider the complexity of the algorithm. In addition, the calculation of these algorithms is very complex, and how to reduce the computational complexity of the algorithms has a great impact on the real-time estimation of the SOC. In an effort to accurately describe the working state of the lithium-ion battery, considering the accuracy and computational complexity of the characterization, an improved UKF algorithm based on reduced-order modeling is used to estimate the SOC of lithium-ion battery, which reduced the computational complexity of the traditional algorithm.

2 Mathematical analysis

2.1 Equivalent circuit modeling

The equivalent circuit model includes the internal resistance model, Thevenin model, PNGV model and so on. The internal resistance model takes the operating characteristics of the battery into account, and the structure is simple. Based on the internal resistance model, Thevenin model introduces the parallel circuit of resistance and capacitance to describe the polarization effect in the battery. It also simulates the dynamic characteristics of the battery. When compared with the PNGV model and the GNL model, the Thevenin model has a simple structure. In addition, it belongs to a nonlinear low-order model. It involves fewer parameters, and its accuracy can meet the requirements of engineering applications. On this basis, the effects of polarization on the voltage and SOC are fully considered, and the Thevenin equivalent circuit model is established to characterize the battery characteristics as shown in Fig. 1.

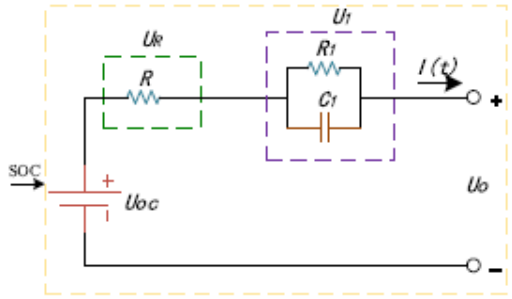

Fig. 1 Equivalent circuit model

In Fig. 1, *U*oc represents the open-circuit voltage. *Uo* represents the terminal voltage. *R* is the ohmic internal resistance, and *UR* is the ohmic voltage, which is the battery voltage drop effect at the end of the discharge. The RC parallel loop is composed of a polarization resistor *R*1 and a polarization capacitor *C*1 for characterizing the polarization effect of the lithium-ion battery.*U*1 is the polarization voltage.

2.2 State-space description

According to Kirchhoff's laws, the Thevenin model is analyzed, and the voltage and current expressions of the equivalent circuit are obtained as shown in Eq. (1):

$$\begin{cases} U_0 = U_{oc} - U_R - U_1 \\ I(t) = C_1 \dfrac{dU_1}{dt} + \dfrac{U_1}{R_1} \end{cases} .$$

Among them, the OCV can be characterized by the state variable SOC, and a nonlinear function can be obtained.

2.3 Three-particle unscented transform

The unscented transformation (UT) is a better method for dealing with nonlinear problems, and it is an important part of the UKF. The fundamental principle is to obtain a finite number of sampling points depending on the statistical characteristics of the state variables and according to a certain sampling method. These points have the same mean and covariance as the original state. In other words, a finite number of points are used to approximate a Gaussian distribution. Then, the Sigma points set is transmitted nonlinearly using the state equation. After that, the transformed mean and covariance are obtained according to a certain weight distribution. SOC is a state variable, and the collection of sampling points is shown in Eq. (2):

$$\begin{cases} \mathrm{SOC}^i = \widehat{\mathrm{SOC}}, i = 0 \\ \mathrm{SOC}^i = \widehat{\mathrm{SOC}} + \left(\sqrt{(n+\lambda)P}\right)_i, \quad i = 1 \sim n \\ \mathrm{SOC}^i = \widehat{\mathrm{SOC}} - \left(\sqrt{(n+\lambda)P}\right)_{i-n}, \quad i = n+1 \sim 2n \end{cases} \tag{2}$$

where n is the dimension of the state variable, λ is the scaling parameter, _SOC is the mean of the state variable and P is the covariance matrix. The corresponding weights are shown in Eq. (3):

$$\begin{cases} \omega_m^0 = \lambda/(n+\lambda) \\ \omega_m^0 = \lambda/(n+\lambda) + \left(1-\alpha^2+\beta\right) \\ \omega_m^i = \omega_c^i = \lambda/2(n+\lambda),\ i = 1 \sim 2n \end{cases} \quad (3)$$

In the formula, $\beta \geq 0$ and is usually 2. In addition, $0 \leq \alpha \leq 1$. k is the auxiliary scale factor. It generally satisfies the following relationship: $\kappa = 3 - n$, $\lambda = \alpha 2\ (n + \kappa) - n$. After that, the original state is transferred backward by using the sampling point

2.4 Improved unscented Kalman filtering

Combined with the Thevenin model and considering the practical application, only the SOC is selected as a system state variable to realize reduced-order modeling. In addition, the terminal voltage $U0$ of the battery is taken as the observed variable of the system. The established battery state space expression is shown in Eq. (4):

$$\begin{cases} \mathrm{SOC}_{k+1} = \mathrm{SOC}_k - I_k \dfrac{\Delta t}{Q_N} + w_k \\ U_{0,k+1} = f\left(\mathrm{SOC}_{k+1}\right) - U_R - U_1 + v_{k+1} \end{cases} \quad (4)$$

In the formula, the SOC value at the time $k + 1$ is predicted at the time k. Δt is the sampling interval time. QN is the rated capacity of the battery, and its actual value is subjected to capacity calibration. Ik is the current. Uoc, k+1 = f ($SOCk$+1) is the relationship between the OCV and the SOC of the lithiumion battery. wk and $vk+1$ are the process noise and observed noise, respectively. The implementation of the improved UKF can be divided into the prediction stage and the update stage. Let the value of the SOCk and the error variance matrix Pk be known. The specific process is as follows.

3 Prediction stage

The estimated value of the system state variable and the error variance matrix at time $k + 1$ are shown in Eq. (5):

$$\begin{cases} \mathrm{SOC}^i(k+1|k) = f\left[\mathrm{SOC}^i(k), u_k\right] \\ \mathrm{SOC}(k+1|k) = \sum_{i=0}^{2n} \omega^i \mathrm{SOC}^i(k+1|k) \end{cases} \quad (5)$$

SOCi(k) is the sampling point obtained by using the unscented transformation. uk is the input variable. SOC(k) is the mean value of the system state. Similarly, the error variance matrix of the time $k + 1$ is predicted as shown in Eq. (6):

$$P(k+1|k) = \sum_{i=0}^{2n} w_c^i \left[\mathrm{SOC}^i(k+1|k) - \mathrm{SOC}(k+1|k)\right] \times \left[\mathrm{SOC}^i(k+1|k) - \mathrm{SOC}(k+1|k)\right]^T + Q_{k+1}. \tag{6}$$

The Sigma sampling points are updated. Substituting the state quantity predicted value point that is set at time $k + 1$ into the observation equation to obtain the observation predicted value at the time $k + 1$ is shown in Eq. (7):

$$\begin{cases} U_0^i(k+1|k) = h\left[\mathrm{SOC}^i(k+1|k), u_k\right] \\ \hat{U}_0(k+1|k) = \sum_{i=0}^{2n} \omega_m^i U_0^i(k+1|k) \end{cases}. \tag{7}$$

The variance matrix of the measured values, the covariance of the state quantity and the measured quantity at the time $k + 1$ are calculated as shown in Eq. (8):

$$\begin{cases} P_{U_0(k+1)U_0(k+1)} = \sum_{i=0}^{2n} \omega_c^i \left[U_0^i(k+1|k) - \hat{U}_0(k+1|k)\right] \times \left[U_0^i(k+1|k) - \hat{U}_0(k+1|k)\right]^T + R_{k+1} \\ P_{\mathrm{SOC}(k+1)U_0(k+1)} = \sum_{i=0}^{2n} \omega_c^i \left[\mathrm{SOC}^i(k+1|k) - \mathrm{SOC}(k+1|k)\right] \times \left[U_0^i(k+1|k) - \hat{U}_0(k+1|k)\right]^T \end{cases}. \tag{8}$$

4 Update stage

The Kalman gain, the update system state variable values and the error variance matrix are calculated as shown in Eq. (9):

$$\begin{cases} K_{k+1} = P_{U_0(k+1)U_0(k+1)} / P_{\mathrm{SOC}(k+1)U_0(k+1)} \\ \mathrm{SOC}(k) = \mathrm{SOC}(k+1|k) + K_{k+1}\left[U_0(k+1) - U_0(k+1|k)\right] \\ P(k+1) = P(k+1|k) - K_{k+1} P_{U_0(k+1)U_0(k+1)} K_{k+1}^T \end{cases}. \tag{9}$$

The improved UKF implementation process is shown in Fig. 2.

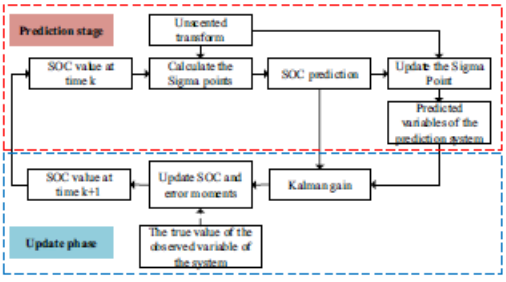

Fig. 2 Improved UKF implementation process

Since the state variable is only one dimension, the number of selected Sigma points is 3. The Sigma point is passed through the system state equation to derive the predicted point group. Then, the Kalman gain and the error between the true value of the observed variable and the prediction are used to continuously correct the predicted value. Finally, the optimal estimate of the system state
variables can be obtained.

5 Experimental analysis

5.1 Test equipment and procedures

An NMC battery with a rated capacity of 50 Ah is selected for the test. The main specifications of the battery are presented in Table 1.

Table 1 Battery specifications

Battery rated capacity	50 Ah
Nominal voltage	3.7 V
Charge limit voltage	4.2 V
Discharge limit voltage	2.75 V
Max. continuous discharge current	200 A

The instruments used in the test include a power cell large-rate charge and discharge tester, a threelayer independent temperature control, high- and low-temperature test chamber and other supporting experimental equipment, as shown in Fig. 3.

Fig. 3 The experimental setup

Since the parameters in the model are affected by temperature, the test is carried out at 27 °C, and the model parameters need to be further improved at high and low temperatures. The battery ages due to recycling and other reasons. Thus, the actual capacity of the battery deviates greatly from the calibration capacity. Therefore, the capacity calibration of the lithium-ion battery must be performed first. In this study, online parameter identification increases the complexity of the algorithm, and the accuracy is not notably improved. Therefore, an offline identification method is selected. The battery is subjected to a pulse discharge experiment, and the battery model parameters are obtained by analyzing the operating characteristics.

5.2 Parameter identification

According to the above experimental steps, the lithium-ion battery capacity is calibrated first. The battery capacity is calibrated as 48 Ah at 27 °C. The pulse discharge test is conducted on the lithium-ion battery. The voltage curve of one of the pulse tests is shown in Fig. 4.

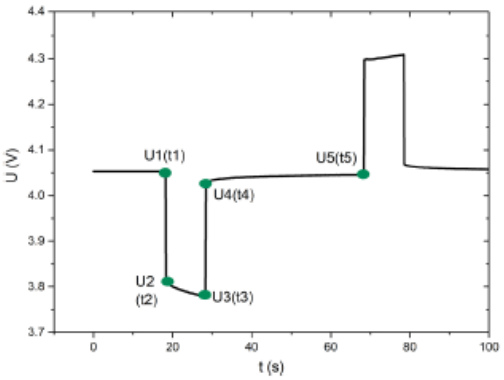

Fig. 4 One-pulse experimental voltage curve

It can be seen from the voltage curve at the end of each constant current discharge in Fig. 4 that the battery will gradually stabilize after a long period of time after the end of the discharge, which means that the internal chemical reaction and thermal effect have basically reached equilibrium. The battery voltage is open-circuit voltage, so the relationship between the OCV and the SOC can be obtained as shown in Fig. 5.

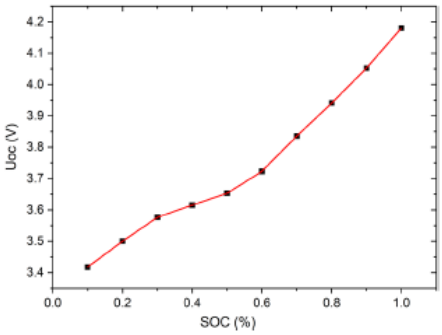

Fig. 5 OCV–SOC relation curve

An analysis of Fig. 4 shows that at the beginning of the discharge from *t*1 to *t*2, the voltage at the battery terminal drops sharply, which yields the ohmic internal resistance of the battery as shown in Eq. (10):

$$R = \frac{|U_2 - U_1|}{I}. \tag{10}$$

In Fig. 4a, when the battery stops discharging at *t*3, the ohm effect disappears and the battery voltage suddenly changes. At the *t*4 ~ *t*5 stage, the battery voltage slowly rises. At this time, it is the zero input effect of the RC circuit in the circuit model. In addition, the battery terminal voltage can be expressed as shown in Eq. (11):

$$U_0 = U_{oc} - IR_1 e^{-\frac{t}{\tau}}. \tag{11}$$

In the formula, the time constant $\tau 1 = R1C1$. The parameters of R, $R1$ and $C1$ of different SOC states are sorted out as shown in Table 2.

Table 2 Parameters

SOC	1	0.9	0.8	0.7	0.6	0.5	0.4	0.3	0.2	0.1
R/mΩ	4.222	4.101	4.083	4.068	4.07	4.083	4.099	4.126	4.179	4.318
R_1/mΩ	1.77	1.81	2.21	2.378	2.262	1.724	1.805	2.076	2.347	3.377
C_1/F	22,341.66	17,754.92	15,107.55	15,161.69	18,362.62	21,121.45	20,470.24	18,674.91	16,295.86	8831.993

The characterization of the battery voltage in the actual operating conditions of the constructed Thevenin model is verified. The real voltage and current data under the cyclic discharge condition are imported into the equivalent model constructed by MATLAB/Simulink. The model is verified by combining with the previous parameter identification results. The estimated value is compared with the actual terminal voltage value, and the comparison result and the corresponding error are shown in Fig. 6a, b, respectively.

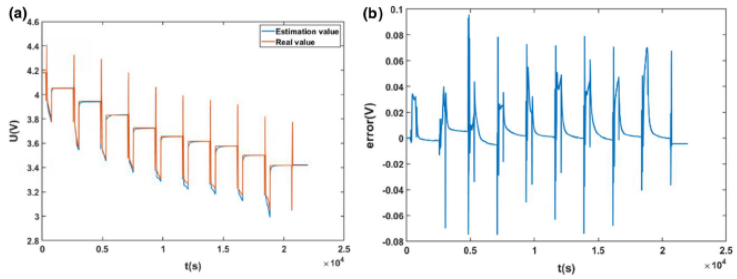

Fig. 6 Thevenin equivalent circuit model simulation: **a** voltage contrast curve; **b** simulation error

Figure 6a shows the comparison between the estimated value of the battery terminal voltage and the true value under the cyclic discharge hold test. The blue solid line is the estimated value based on the constructed model, and the red solid line is the actual battery terminal voltage value. Figure 6b shows the variation of the simulation error. It can be seen from the figure that the estimated value has a good tracking effect on the true value. In addition, the average estimated deviation is about 0.03 V, which can characterize the value of the terminal voltage of the battery during operation. The analysis of the voltage comparison error shows that the voltage estimation error increases at the end of the battery discharge. On the one hand, the battery voltage changes dramatically at the end of the discharge, and the estimated value of the simulation lags behind the effect, which leads to a larger estimation error. On the other hand, it shows that the Thevenin model has shortcomings in characterizing the battery operating characteristics.

5.3 Dynamic working condition analysis

In order to verify the overall performance of the improved UKF algorithm in actual application, the accuracy, convergence and traceability of the model are studies under various experimental conditions. The current pulse discharge experiment and an experiment under dynamic stress test (DST) conditions are performed on the estimated models.

5.3.1 Current pulse discharge experiment

Considering that the battery is often in an intermittent discharge state in actual use, the model is further simulated and analyzed under the conditions of current pulse discharge.
The experimental results are shown in Fig. 7.

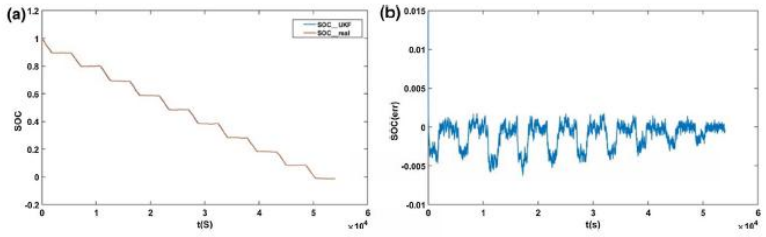

Fig. 7 Improved UKF-SOC estimation and estimation error under cyclic discharge: **a** UKF-SOC estimation; **b** simulation error

Figure 7a shows the actual SOC and the estimated value of the improved UKF. It can be seen from the figure that the improved UKF algorithm converges and that the tracking effect is good. When estimating the initial algorithm to quickly converge, the required time is about 100 s to track the theoretical value. The estimated deviation is stable and within 0.7%. In addition, the overall performance is excellent. It is proved that the improved UKF has good convergence and tracking performance for SOC estimation. It is worth noting that when the battery is in a suspended state, the SOC estimation error becomes larger. This is due to the fact that when the battery is in a suspended state, there is a lag in the battery equivalent circuit model, which results in a failure to obtain the real-time and accurate battery terminal voltage.

5.3.2 Dynamic stress test condition experiment

In order to further verify the response of the model to the SOC of the lithium-ion battery under more complicated application conditions, the model is simulated and verified by experimental data of a customized DST condition. The DST working condition is more complicated and can better reflect the working status of lithium batteries. Under the same working condition, the Ah integral and the UKF algorithm are added to perform synchronous simulation analysis to compare the advantages of the improved UKF algorithm. The experimental voltage and current data of the DST working condition are shown in Fig. 8.

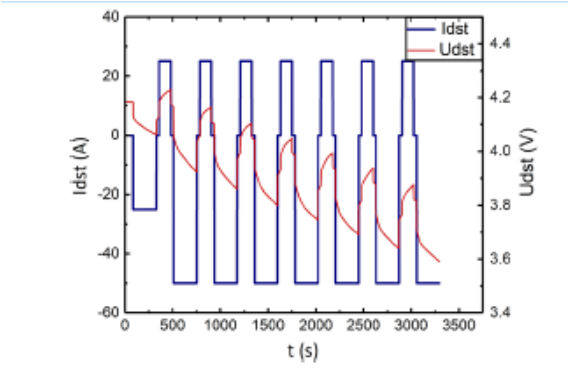

Fig. 8 Voltage and current curves of the DST working condition

The results of comparing the SOC with the real value and the estimation error using Ah, UKF and the improved UKF are shown in Fig. 9.

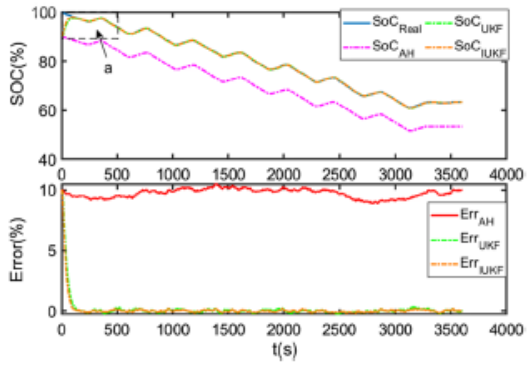

Fig. 9 SOC and estimation error under the DST condition

In order to compare the estimated effects of the traditional UKF and the improved algorithm, the estimated SOC curve is partially enlarged and shown in Fig. 10. In order to verify the convergence effect of the algorithm in the estimation process and the tracking of the real value, the initial value of the algorithm is set to 0.9. The error results obtained by several algorithms for estimating SOC are shown in Table 3.

Table 3 Estimation error

Algorithm	Average error	Convergence time (unit:s)
Ah	8%	–
UKF	0.2%	160
IUKF	0.1%	130

Under the DST condition, in the initial stage of estimation, the Ah integral method cannot quickly converge to track the true value, and the estimation error is much larger than those of the others. In addition, the error becomes larger as the estimation time increases. Both the UKF and the improved algorithms are able to track the real SOC values, and they are stable at the end of the estimation. However, from the SOC estimation partial enlargement in Fig. 10 and the estimation error comparison in Fig. 9, it can be seen that the IUKF can converge to the true value more quickly. The estimation error is kept within 0.2%. This verification illustrates the superiority of the improved UKF in estimating lithium-ion battery SOC.

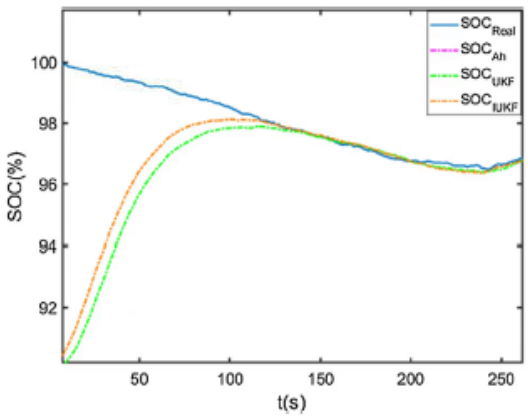

Fig. 10 SOC and estimation errors of AH, UKF and IUKF under the DST condition

Conclusions

It is important and difficult to accurately estimate the SOC of lithium-ion batteries. In this paper, Thevenin model was used to characterize the state and output characteristics of the lithium-ion battery, where the pulse discharge experiment was conducted to identify the parameters. In addition, the relationships between the circuit model parameters and the SOC of the lithium-ion battery in different discharge stages were also determined. On this basis, the traditional Kalman algorithm was improved. The improved algorithm reduced the complexity of the traditional algorithm by constructing a reduced-order model and can quickly estimate the SOC of the battery. The Simulink model was established on MATLAB and combined with experimental data under variousworking conditions for analysis. The results show that the improved UKF algorithm can estimate the SOC of the lithium-ion battery well. They also showed that the estimation error can be controlled within 0.5%, which verifies that the improved UKF has a high accuracy in the SOC estimation of lithium-ion batteries.

Acknowledgements

The work was supported by National Natural Science Foundation of China (No. 61801407).

References

1. Qin, Y.C., et al.: Noise and vibration suppression in hybrid electric vehicles: State of the art and challenges. Renew. Sustain. Energy Rev. (2020). https://doi.org/10.1016/j.rser.2020.10978 2
2. Bian, X.L., Liu, L.C., Yan, J.Y.: A model for state-of-health estimation of lithium ion batteries based on charging profiles. Energy **177**, 57–65 (2019)
3. Yang, J.F., et al.: Adaptive state-of-charge estimation based on a split battery model for electric vehicle applications. IEEE Trans. Veh. Technol. **66**(12), 10889–10898 (2017)
4. Liu, T., et al.: Adaptive hierarchical energy management design for a plug-in hybrid electric vehicle. IEEE Trans. Veh. Technol. **68**(12), 11513–11522 (2019)
5. Mandli, A.R., et al.: Fast computational framework for optimal life management of lithium ion batteries. Int. J. Energy Res. **42**(5), 1973–1982 (2018)
6. Fridholm, B., et al.: Estimating power capability of aged lithium-ion batteries in presence of communication delays. J. Power Sources **383**, 24–33 (2018)
7. Rosewater, D., et al.: Battery energy storage state-of-charge forecasting: models, optimization, and accuracy. IEEE Trans Smart Grid **10**(3), 2453–2462 (2019)
8. Misyris, G.S., et al.: State-of-charge estimation for li-ion batteries: a more accurate hybrid approach. IEEE Trans. Energy Convers. **34**(1), 109–119 (2019)
9. Ouyang, M.G., et al.: Progress review of US-China joint research on advanced technologies for plug-in electric vehicles. Sci. China-Technol. Sci. **61**(10), 1431–1445 (2018)
10. Li, S.X., et al.: Fractional-order modeling and SOC estimation of lithium-ion battery considering capacity loss. Int. J. Energy Res. **43**(1), 417–429 (2019)
11. Gao, Y.Z., et al.: Estimation of state-of-charge and state-ofhealth for lithium-ion degraded battery considering side reactions. J. Electrochem. Soc. **165**(16), A4018–A4026 (2018)
12. Zhang, Z.L., et al.: SOC estimation of lithium-ion battery pack considering balancing current. IEEE Trans. Power Electron. **33**(3), 2216–2226 (2018)
13. Liu, D.T., et al.: Hybrid state of charge estimation for lithiumion battery under dynamic operating conditions. Int. J. Electr. Power Energy Syst. **110**, 48–61 (2019)
14. Wang, T.P., et al.: Model-based unscented Kalman filter observer design for lithium-ion battery state of charge estimation. Int. J. Energy Res. **42**(4), 1603–1614 (2018)

15. Feng, F., et al.: Online estimation of model parameters and state of charge of LiFePO4 batteries using a novel open-circuit voltage at various ambient temperatures. Energies **8**(4), 2950–2976 (2015)
16. Sturm, J., et al.: State estimation of lithium-ion cells using a physicochemical model based extended Kalman filter. Appl. Energy **223**, 103–123 (2018)
17. Kim, T., Qiao, W., Qu, L.Y.: An enhanced hybrid battery model. IEEE Trans. Energy Convers. **34**(4), 1848–1858 (2019)
18. Saldana, G., et al.: Analysis of the current electric battery models for electric vehicle simulation. Energies. (2019). https ://doi.org/10.3390/en121 42750
19. Wei, Z.B., et al.: Comparative study of methods for integrated model identification and state of charge estimation of lithium-ion battery. J. Power Sources **402**, 189–197 (2018)
20. Kim, T., et al.: An on-board model-based condition monitoring for lithium-ion batteries. IEEE Trans. Ind. Appl. **55**(2), 1835–1843 (2019)
21. Shrivastava, P., et al.: Overview of model-based online stateof-charge estimation using Kalman filter family for lithiumion batteries. Renew. Sustain. Energy Rev. (2019). https ://doi.org/10.1016/j.rser.2019.06.040
22. Talha, M., Asghar, F., Kim, S.H.: A neural network-based robust online SOC and SOH estimation for sealed lead-acid batteries in renewable systems. Arab. J. Sci. Eng. **44**(3), 1869–1881 (2019)
23. Bester, J.E., El Hajjaji A., Mabwe, A.M.: 41st Annual Conference of the IEEE-Industrial-Electronics-Society (IECON). Modelling of lithium-ion battery and SOC estimation using simple and extended discrete Kalman filters for aircraft energy management.
Iecon 2015—41st Ann. Yokohama, JAPAN, pp 2433–2438 (2015)
24. Wu, T.Z., et al.: Voltage-SOC balancing control scheme for seriesconnected lithium-ion battery packs. J. Energy Storage. (2019).
https ://doi.org/10.1016/j.est.2019.10089 5
25. Zheng, L.F., et al.: Differential voltage analysis based state of charge estimation methods for lithium-ion batteries using extended Kalman filter and particle filter. Energy **158**, 1028–1037 (2018)
26. Wu, X.G., Li, X.F., Du, J.Y.: State of charge estimation of lithiumion batteries over wide temperature range using unscented Kalman filter. IEEE Access **6**, 41993–42003 (2018)
27. Afshar, S., Morris, K., Khajepour, A.: State-of-charge estimation using an EKF-based adaptive observer. IEEE Trans. Control Syst. Technol. **27**(5), 1907–1923 (2019)
28. Li, L.L., Liu, Z.F., Wang, C.H.: The open-circuit voltage characteristic and state of charge estimation for lithium-ion batteries based on an improved estimation algorithm. J. Test. Eval. **48**(2), 1712–1730 (2020)
29. Xu, Y.D., et al.: State of charge estimation for lithium-ion batteries based on adaptive dual Kalman filter. Appl. Math. Model. **77**, 1255–1272 (2020)
30. Li, B., Bei, S.Y.: Estimation algorithm research for lithium battery SOC in electric vehicles based on adaptive unscented Kalman filter. Neural Comput. Appl. **31**(12), 8171–8183 (2019)
31. Guo, F., et al.: A multi-scale parameter adaptive method for state of charge and parameter estimation of lithium-ion batteries using dual Kalman filters. Energy **178**, 79–88 (2019)
32. Wang, S.L., et al.: Adaptive state-of-charge estimation method for an aeronautical lithium-ion battery pack based on a reduced particleunscented Kalman filter. J. Power Electron. **18**(4), 1127–1139 (2018)
33. Mawonou, K.S.R., et al.: Improved state of charge estimation for Li-ion batteries using fractional order extended Kalman filter. J. Power Sour. (2019). https ://doi.org/10.1016/j.jpowsour.2019.22671 0